Europe PMC Funders Group
Author Manuscript
Nat Commun. Author manuscript; available in PMC 2016 February 18.

Published in final edited form as:
Nat Commun. ; 6: 8009. doi:10.1038/ncomms9009.

Directing cell therapy to anatomic target sites *in vivo* with magnetic resonance targeting

Munitta Muthana[1,*], **Aneurin J Kennerley**[#2], **Russell Hughes**[3], **Ester Fagnano**[1], **Jay Richardson**[1], **Melanie Paul**[1], **Craig Murdoch**[4], **Fiona Wright**[1], **Christopher Payne**[6], **Mark F. Lythgoe**[6], **Neil Farrow**[7], **Jon Dobson**[8], **Joe Conner**[9], **Jim M Wild**[5], and **Claire Lewis**[3]

[1]Department of Infection and Immunity, University of Sheffield, Sheffield, S102RX, UK

[2]Department of Psychology, University of Sheffield, Sheffield, S102RX, UK

[3]Department of Oncology, University of Sheffield, Sheffield, S102RX, UK

[4]Unit of Oral & Maxillofacial Medicine & Surgery, University of Sheffield, Sheffield, S102RX, UK

[5]Cardiovascular Sciences, University of Sheffield, Sheffield, S102RX, UK

[6]Centre for Advanced Biomedical Imaging, Division of Medicine, University College London, London, WC1E 6DD, UK

[7]Institute for Science & Technology in Medicine, Keele University, Stoke-on-Trent, ST4 7QB, UK

[8]Department of Biomedical Engineering, University of Florida, Gainesville, Florida, FL 32611

[9]Virttu Biologics, Glasgow, Glasgow City, G51 4TF, UK

[#] These authors contributed equally to this work.

Abstract

Cell-based therapy exploits modified human cells to treat diseases but its targeted application in specific tissues, particularly those lying deep in the body where direct injection is not possible, has been problematic. Here we use a magnetic resonance imaging (MRI) system to direct macrophages carrying an oncolytic virus, Seprehvir, into primary and metastatic tumour sites in mice. To achieve this, we magnetically label macrophages with super-paramagnetic iron oxide nanoparticles (SPIOs) and apply pulsed magnetic-field gradients in the direction of the tumour sites. Magnetic resonance targeting guides macrophages from the bloodstream into tumors, resulting in increased tumour macrophage infiltration and reduction in tumor burden and metastasis. Our study indicates that clinical MRI scanners can not only track the location of magnetically labelled cells but also have the potential to steer them into one or more target tissues.

Users may view, print, copy, and download text and data-mine the content in such documents, for the purposes of academic research, subject always to the full Conditions of use:http://www.nature.com/authors/editorial_policies/license.html#terms

[*]corresponding author, m.muthana@sheffield.ac.uk.

Author contributions

MM, AK, RH, EF, JR, MP, FW, CP performed the experiments. MM, AK, CM, MFL, CPNF, JD, JMW, CL helped design the experiments and analysed the data. MM wrote the manuscript with contributions from all authors. JC provided the virus Sepraphir and helped design the experiments using this virus.

Competing financial interest

The authors declare no competing interests.

Europe PMC Funders Author Manuscripts
Europe PMC Funders Author Manuscripts

Europe PMC Funders Author Manuscripts

Europe PMC Funders Author Manuscripts

Introduction

Advances in our understanding of the molecular mechanisms underpinning major diseases have led to the development of a wide array of cell-based therapies to deliver a therapeutic agent like a protein or virus, or a modified, repopulating stem cell[1]. When the disease is not confined to one site in the body, or is in a tissue inaccessible by direct injection of cells, such cell-based therapies have to be administered systemically.

Previous studies have shown that magnetic particles or cells loaded with SPIOs can be injected systemically and attracted to a target tissue in mice by the application of a local external magnet[2-6]. Indeed, we have previously showed that SPIO-loaded human macrophages could be attracted from the circulation into tumors in mice using such an approach[7]. However, this approach can only be applied to superficial target tissues. While localised magnetic field gradients could be achieved in deeper tissues using implanted ferromagnetic stents[8], this necessitates invasive surgery.

An exciting, alternative approach is magnetic resonance targeting (MRT) which uses the magnetic field gradient coils inherent to all magnetic resonance imaging (MRI) systems, to steer ferromagnetic particles (or cells containing them) to a target site[4]. We have previously shown that MRI could be used to steer iron-labeled human PBMCs in a vascular model[7], and early studies in pigs demonstrated this concept by steering a 1.5mm ball bearing a distance of 5cm inside the right carotid artery of the animal using the gradient coil currents of a standard 1.5 T MRI system[9,10].

Bone marrow-derived cells (BMDCs) are increasingly being used in cell-based therapies for such diseases as infarcted myocardium[11], spinal cord injury[12], cerebral ischemia[13], degenerative diseases like Parkinson's Disease[14], Alzheimer's Disease[15] and cancer[16-18]. In the latter disease, numerous clinical trials have administered bone marrow-derived cells systemically in an attempt to treat malignant tumors, including T-cells[19,20], dendritic cells[21], macrophages[22,23] and stem cells[24]. However, only a small proportion of these cells subsequently locate to the tumor site, with many found subsequently in other tissues. This lack of targeting not only reduces the therapeutic efficacy but also increases the risk of side effects.

When macrophages were found to accumulate in large numbers in avascular hypoxic/necrotic areas of such tissues in mice and humans[17,25,26] we suggested that these cells could be used to deliver therapeutic agents like oncolytic viruses (OV) to these poorly vascularized, and therefore relatively inaccessible, areas of tumors[17]. In the present report, we show that MR targeting can be used to increase the number of OV-loaded macrophages in primary and metastatic tumors in mice. Importantly, MR targeting markedly increased the anti-tumor effects of this macrophage virotherapy. Our results suggests that it is possible to use a standard MRI scanner to non-invasively steer cells to both primary and secondary tumors, and so, in theory, this approach could be used to steer any cell-based therapy to its target site(s) within the body.

Europe PMC Funders Author Manuscripts

Europe PMC Funders Author Manuscripts

Results

MR targeting of magnetic cells into 3D tumour spheroids

Before applying MR targeting techniques *in vivo* we first established that a pre-clinical 7T MRI system fitted with a 600mT/m gradient coil (limited to ~300mT per m for this study) set could generate substantial actuation forces on magnetic macrophages *in vitro* by steering them across an endothelial layer into 3D human multi-cellular tumor spheroids (MTS). To do this, we designed a trans-endothelial migration (TEM) flow chamber in which human macrophages circulated across the surface of a perforated membrane coated with a layer of human vascular endothelial cells, thereby mimicking flow in tumor venules. MTS were cultured in a non-adherent chamber below the membrane (Fig. 1a). Human macrophages transfected to express a GFP reporter adenovirus (Ad-CMV-GFP) were loaded with SPIOs (1.18ug per ml ± 0.3)[7] and then steered across the membrane into MTS when the chamber was placed in the iso-centre of a pre-clinical MRI system.

MR targeting (MRT) experiments used a pulsed magnetic field gradient (2 ms on, 7 ms off, 50% strength ~300mT per m^4) for 1 hour in the direction of the spheroids (Fig. 1a) with an effective additional magnetic field offset, B_{off} ~ +1.5mT around the MTS site. In control conditions samples were exposed to the magnetic field of the scanner but gradients were not pulsed. Following MRT, we found a T_2*-weighted signal loss indicating higher concentration of iron in comparison to the control samples for MRT samples (n=6) (Fig 1.c, **upper panel**). GFP-expressing macrophages were also clearly visible within MTS (Fig 1.c, **2nd panel**) and flow analysis further confirmed macrophage uptake with significantly more viable infiltrating $CD14^+/PI^-$ expressing macrophages with MR targeting (29.7%±2.6) than without (2.9%±1.8) (Fig. 1 c, **lower panel**).

MRT improves tumour uptake of magnetic cells *in vivo*

We then investigated whether such an MRI gradient system could be used to steer magnetic macrophages to tumors *in vivo* (Fig. 2). Three million SPIO-loaded macrophages were administered intravenously to mice bearing orthotopic primary and metastatic (lung) prostate tumors. A pulsed magnetic field gradient[4] was applied for 1 hour, in the direction of the prostate (Fig. 2a), with an effective magnetic field offset, B_{off} ~ +7mT on top of the static magnetic field of the scanner (B_0 = 7T). The control group were exposed to the static magnetic field of the scanner in the absence of the steering gradients (no MR targeting).

MR targeting significantly (unpaired student t-test p=0.0001) increased uptake of SPIO-loaded macrophages in primary prostate tumors (42.2%±2.5) compared to the control group who did not undergo MR targeting (7.17%±0.8) (Fig. 2b). Moreover, we observed these SPIO+ human macrophages were distributed throughout tumors with very few signs of cell clumping in the tumor vasculature following MR targeting as seen by labeling sequential sections of tumors using an antibody against human CD68 (a pan macrophage marker) and a histological stain for iron (Prussian Blue or ‘PB’) (Fig. 2c). This was also confirmed by immunofluorescence staining where tumor cells are labelled with the anti-GFP antibody (green) and tumor infiltrating human macrophages with anti-CD68 (red) (Supplementary Fig. 1a). MRI steering of macrophages did not adversely affect the tumor vasculature

Europe PMC Funders Author Manuscripts

Europe PMC Funders Author Manuscripts

(Supplementary Fig. 1b); we examined the morphology and integrity of every CD31+ blood vessel in each of the 5 tumors in these 2 groups and found no differences between them. We could not see signs of endothelial cell disruption, nor were there any signs of blood clotting (e.g. platelet aggregation) in, or on the abluminal side of blood vessels after MRI targeting. In the multi-echo RARE MR images of tumors little difference can be seen between the MR targeting and no MR targeting groups (Fig. 2d). This is most likely due to the blood pool iron content per voxel. However, a marked difference between SPIO injected and non-injected subjects is evident in the T2-weighted long TE images, with loss in signal intensity within the tumor indicating the presence of high concentrations of iron (Fig. 2e). In an effort to assess the increased uptake of magnetic macrophages *in vivo* we used MR relaxometry to measure the MR transverse relaxation decay rate (R_2) in tumors in both groups. R_2 measurements were $21.8s^{-1}$ for the MR targeting group and $18.8s^{-1}$ for the control group. Normal R_2 decay rate of tumor tissue without the presence of any SPIOs is also included for comparison ($10.5s^{-1}$). The increased R_2 decay rate indicated increased iron uptake for the MR targeting group, suggesting it is possible to assess the uptake with MRI, as seen with the post mortem analysis (Supplementary Fig. 1c). The difference in targeted and non-targeted R_2 values was used to estimate the optimal echo time for analysing signal differences with spin echo-based MRI sequences (TE of 60ms). Using this TE, MR targeting leads to a 10% decrease in signal over the time-matched controls.

Additional controls included tumor-bearing mice: (i) with unlabelled macrophages and MR targeting, and (ii) with unlabelled macrophages without MR targeting. For these control groups, we detected very few macrophages within tumors as confirmed by MRI imaging (Supplementary Fig. 1d) and flow cytometry of enzymatically dispersed tumors (Supplementary Fig. 1e). Of note, we detected virtually no human CD68+ macrophages in other tissues including the liver (<2% of all cells per tissue section), spleen (<1%) and kidneys (none detected) (Supplementary Fig. 2).

To further investigate if macrophage delivery to tumours by MRT disrupted the function or integrity of the tumour vasculature, vascular perfusion and permeability was determined using i.v. tomato lectin and *Ricinus communis* agglutinin I staining respectively[27]. We could not detect any differences in the number of perfused vessels or vascular leakage between the no MRT and +MRT groups (Fig. 2f). This was confirmed by estimating vascular permeability to gadolinium-diethylenetriaminepentaacetic acid (Gd-DTPA) by dynamic contrast-enhanced (DCE) MRI (Fig. 3).

MR Targeting of magnetic cells to pulmonary metastasis

MR targeting has particular application when tumors are difficult or impossible to remove surgically, as in the lung, brain, liver or spinal cord and may enable delivery of cell-based therapies to primary or metastatic tumors in such locations. In a second *in vivo* experiment we used MR targeting to steer SPIO-labelled macrophages into the lungs of our mice bearing metastatic prostate tumors (Fig. 4). This was done immediately after i.v. administration of 3 million macrophages. Mice not exposed to MR targeting, but exposed to the magnetic field of the scanner for the same length of time, were used as controls.

Europe PMC Funders Author Manuscripts

Europe PMC Funders Author Manuscripts

Flow cytometric analysis of enzymatically dispersed lungs showed the presence of significantly more human CD14+ macrophages following MR targeting than in the control group (17.7%±4 vs. 4.4%±2.6, respectively) (Fig. 4a). This was also confirmed by histological and immunofluorescence staining of lungs, where human CD68+ macrophages were detected in or close to the small metastatic deposits present within the lungs of mice following MR targeting (Fig. 4b and Supplementary Fig. 3a). These macrophages also stained positive for PB (iron) (Fig. 4b) and their iron content was also visible following H&E staining (Supplementary Fig. 3b). We inspected the morphology of CD31+ blood vessels in the lungs following their uptake of SPIO-labelled macrophages with or without MRT (Fig. 4c). Due to the short T2/T2* of lung tissue it was not possible to image the lung parenchyma with conventional ^{1}H MRI techniques at high field for *in vivo* validation of increased uptake. Future technical developments may make this possible, for example the use of hyperpolarised gases in the airspaces could be used as an indirect MR signal detection method[28]. Nevertheless, in different organs or soft tissues, or on clinical systems, T2* imaging may have a place.

MR targeting of oncolytic macrophages reduces tumor growth

In a final experiment to assess the therapeutic benefits of MR targeting, SPIO-loaded macrophages armed with the OV, Seprehvir (HSV1716), were administered to tumor bearing mice. HSV1716 replication is supported by PC3 prostate cancer cells[29] and here we show, for the first time, oncolysis in LNCaP cells in both hypoxic (0.5% O_2) and normoxic (20%O_2) conditions (Supplementary Fig. 4a). Seprehvir is readily taken up by macrophages and whilst uptake is significantly higher in normoxic culture conditions (Supplementary Fig. 4b), viral replication is greater in hypoxia and macrophage cell death is equally effective in a hypoxic environment (Supplementary Fig. 4c,d). In our *in vivo* model, tumor-bearing mice received either a single intravenous injection of OV-carrying macrophages (MDM+OV), were placed in the static field of the scanner without MR targeting ‘MDM+OV(noMRT)’, or were exposed to the scanner with MR targeting (MDM+OV+MRT). For the purpose of comparison “free” OV was administered to a separate group of mice. Additional control groups of mice received either 100ul saline treatment (Control) or 3 million untreated macrophages (MDM) intravenously. OV (1×10^{7} pfu)[29] alone significantly delayed primary tumor growth for up to 7 days compared to mice receiving PBS or MDM only (Fig. 5a). This effect was significantly prolonged with macrophage-mediated delivery of Seprehvir ($p < 0.006$ at day 14 and $p<0.007$ day 21, a one-way ANOVA followed by post-hoc Bonferroni test was used for statistical analysis) and concurred with our previous studies where macrophages carrying OV were more effective over viral infusion alone[17,18]. Of note, no differences were observed in mice receiving MDM+OV but were not exposed to the MRI scanner and MDM+OV (no MRT) where the latter is exposed to the scanner but with no steering. However, MR targeting of our macrophage virotherapy was not only better at reducing the growth of the primary tumors from day 7 onwards, but also delayed primary tumor regrowth for the entire experiment (Fig. 5a). Bioluminescence of mice receiving macrophage OV therapy with or without MR targeting on the first day of treatment (day 0) and at the end of the experiment (day 21) showed this marked reduction of the primary tumor (Fig. 5a&b). This was confirmed visually on the MRI scans (Fig. 5c). Furthermore,

Europe PMC Funders Author Manuscripts

Europe PMC Funders Author Manuscripts

tumors undergoing MR targeting following macrophage-delivered OV were significantly more necrotic than those not receiving MR targeting (Fig. 5d).

In the lungs, few metastases were detected in mice injected with PBS or MDM alone since mice had to be culled at day 14 (due to the large size of their primary tumors). Therefore, it was not valid to compare metastases in these control groups with the other experimental groups. However, as shown in Fig. 5e the number of lung metastases was markedly reduced in mice that received MR targeted, OV-bearing macrophages than in those which received the cells but not MR targeting.

Discussion

In this study we show that an MRI scanner can be used to non-invasively steer cells to both primary and secondary tumors within the body leading to a significant improvement in therapeutic outcome. Moreover, relaxometry measurements suggest that standard MR imaging can then be used to monitor the efficacy of this therapy. Whilst this study has focused on cell delivery to tumors, the technology could be used to target any cells (e.g. mesenchymal stem cells, etc.) to a given tissue in the body including non-phagocytic cell types which could be ‘magnetised’ using SPIO-conjugated antibodies directed against proteins on their cell surface (Fig. 6).

The use of magnetic resonance targeting, which exploits the magnetic field gradients within magnetic resonance imaging systems to increase delivery of cells, is ideally suited to deep or superficial tissue[7]. The question of clinical translation is dependent on the ability to provide the same targeting force on a clinical MRI system. Clinical scanners, with high performance magnetic field gradient systems of 300mT m^{-1}, are already in use and as such have the potential to produce similar forces[30]. Moreover, we were able to image the cell distributions following MRT, indicating the possibility for real-time image-guided targeting using an MRI system. These findings support the potential value of MRT with concomitant imaging for improved targeting of cells for therapy.

Materials and Methods

Isolation and culture of human macrophages

All patients donating blood gave informed consent to the Sheffield blood Transfusion Service and all procedures have been approved by the University of Sheffield Ethics Committee. Mononuclear cells were isolated from platelet-depleted buffy coats (Blood Transfusion Service, Sheffield, UK) using Ficoll-Paque Plus (Amersham Pharmacia, St. Albans, UK). In brief, fifty million monocytes were plated into T75 tissue culture flasks (NUNC, UK) and after 2 h non-adherent cells were removed. The remaining adherent cells were cultured over 7 days in IMDM Medium (Lonza, UK) supplemented with 2 mmol L^{-1} L-glutamine, 100 U mL^{-1} penicillin, 100 μg mL^{-1} streptomycin, and 2% human Ab serum (Lonza).

Europe PMC Funders Author Manuscripts

Europe PMC Funders Author Manuscripts

Endothelial cell cultures

Human Umbilical Vein Endothelial Cells (HUVEC) were obtained from Promocell, (Heidelberg, Germany) and used in the experiments up to passage 8. Cells (150,000) were seeded for 24h onto collagen-coated (0.1 mg/ml, human type IV) membranes containing a 5 μM pore PET membrane (Neuroprobe).

Human multi-cellular tumor spheroids

Human prostate cancer cell line, LNCaP (ATCC CRL-1740), were seeded (5×10^3) in 100 μl medium into each well of a 2% agarose (Sigma, Dorset, UK) coated 96-well tissue culture plate. After 7–10 days, each well contained a tumor spheroid with an average diameter of 700-800 μm.

Infection of primary macrophages

Day 3 MDMs were infected with a replication deficient adenovirus (CMV-AdV5-GFP) at MOI 100. The E1A/B-deleted adenoviral vectors, CMV-AdV5-GFP (driven by a CMV promoter) was isolated from a single plaque, expanded in 293 human embryonic kidney (HEK) cells All the viruses were purified by double caesium gradient centrifugation, and titered by plaque assay on 293 cells with the titer expressed as plaque forming units (PFU)/ cell. The MOI used in this study were previously optimized in macrophages and are described in[17].

Cellular uptake of magnetic nanoparticles by macrophages

MDMs (infected with AdCMV-GFP) were cultured overnight with 100 μg/ml SPIOs (25 nm) (Sigma-Aldrich, Poole, UK). SPIO accumulation in cells was previously assessed by flow cytometry and confirmed by attraction of the cells towards a magnet placed at the side of the culture dish as observed by light microscopy (Leica Microsystems UK Ltd). Cell viability following SPIO uptake by macrophages was also measured by flow cytometry and compared to cells that were not incubated with SPIOs using the DNA dye propidium iodide (PI, Sigma). Comparisons made using an unpaired student t-test revealed no statistically significant difference between the two groups p=0.4 (Supplementary Fig. 1b) N=3.

In vitro trans-endothelial flow assay

The trans-endothelial migration (TEM) chamber was assembled as shown in (Fig. 1a). SPIO-loaded MDM (1.5×10^5 cells/ml in PBS + 2% FCS) were flowed over the HUVEC monolayer at typical venous flow rates (1.1885 ml/min) at a sheer stress of 1.4 Dynes/cm^2, this is equivalent to blood flow through post-capillary venules. The TEM chamber was positioned directly in the iso-centre at ~5mm distal of a 7 Tesla magnet (Bruker BioSpecAVANCEII, 310mm bore, MRI system B/C 70/30). The flow in the chamber was in the −z direction (in and out of the magnet bore). We used pulsed gradients 2 ms on, 7 ms off as described by Reigler et.al[4]. To steer SPIOs into the chamber containing tumor spheroids we applied a pulsed −y gradient at 50% strength to avoid over-heating (~300mT/m) for 30 minutes. Post MR targeting a ^{1}H volume resonator (Bruker, 300MHz, 1kW max, outer diameter 118mm per inner diameter 72mm) allowed capture of MR images (FLASH and RARE).

Europe PMC Funders Author Manuscripts

Europe PMC Funders Author Manuscripts

Spheroid infiltration by MDMs was then assessed using a fluorescent microscope to detect the GFP positive cells and flow cytometry using enzymatically-dispersed spheroids. To determine the iron content within SPIO-loaded macrophages, cell pellets were solubilized in 70% nitric acid for 7–14 days prior to analysis. Iron concentrations were quantified against a calibration standard iron solution (Fischer Scientific) by Atomic Emission Spectroscopy using Varian Vista-M PX.

Flow cytometric analysis

Single cell suspensions were obtained by trypsinizing MDMs (including co-transduced MDMs). Cells were then incubated with for 30 min at 4°C with mouse anti-CD14, 1:100 in PBS containing 1% BSA (Sigma) to prevent non-specific antibody binding. Alternatively, spheroids were digested using 0.25% trypsin/EDTA to separate the tumor cells and infiltrated macrophages and cell death was analyzed by flow cytometry by adding propidium iodide (Sigma) to the cells immediately before running on the flow cytometer.

Orthotopic prostate xenograft model

All mouse procedures were conducted in accordance with the UK Home Office Regulations under the Animals (Scientific Procedures) Act 1986 and the awarded project licence number under which these protocols were performed is PPL:40/3424. In addition the University of Sheffield Animal Welfare & Ethical Review Body approved all the in vivo experiments used in this study. Male CD1 athymic mice (aged 7-8 weeks, stock number 000711) were used in these studies (Charles Rivers, UK). Animals were randomized before beginning the treatment schedule and were kept in ventilated cages with food and water provided ad libitum. Animal group sizes were calculated by power analysis. In general, a maximum of 5 animals per group were used unless otherwise stated. One million LNCaP:LUC:GFP cells (a gift from Professor Magnus Essand, Uppsala Sweden) were mixed 1:1 in Matrigel and injected into the dorsolateral prostate. Tumor size was determined by administering luciferin (Molecular Probes) followed by bioluminescent IVIS imaging and measuring the daily weights of the mice. Tumor take was monitored by bioluminescence imaging using the IVIS Lumina II imaging system (Caliper Life Sciences). This detects live luciferase-labeled tumor cells, enabling real-time monitoring of tumor growth and spread in the mice. The mice were injected intraperitoneally (i.p.) with 90 mg/kg D-luciferin (Caliper Life Sciences) dissolved in sterile water and anaesthetized using 2.5% isoflurane (Abbott Scandinavia AB) in 100% oxygen at 3.5 L/min (for induction) in the anesthesia chamber of the imaging system. Mice were transferred to the dark box and isoflurane was lowered to 1.5%. Images were taken every 3 minutes as a sequence of 10 images for every group of mice, once a week. Automatic contour regions of interest were created, and the tumor sizes (or tumor radiance) were quantified as photons per second per square centimeter per steradian (ps^{-1}per cm^2 per sr^1). Progression and spread of tumors were evaluated by calculating the tumor radiance values from inoculated mice in each group. Tumor-bearing mice were used in experiments approximately 14 days following implantation or 21 days in the metastases model when the pulmonary tumors develop following orthotopic implantation of the tumor cells into the prostate[17]. Mice not developing tumors were excluded from the experiments (<5%). All mice were closely monitored and any displaying signs of rapid weight loss, excessively

Europe PMC Funders Author Manuscripts

Europe PMC Funders Author Manuscripts

large tumours (>10^{10} ps-1, or 15 mm in diameter) or any pain/suffering/distress sufficient to impede natural behavior were culled.

Use of the MRI scanner to direct cell movement

Three million MDMs with or without SPIOs were administered via tail vein in 100μl volume of PBS (n=5), control groups received 100ul PBS (n=5), or 100ul PBS containing 3 × 10^6 macrophages without SPIOs (n=5). Immediately after MDM administration mice were anaesthetized with gaseous isoflurane (Abbott, UK) and then secured within a magnet-compatible holding capsule and MR targeting was carried out immediately using a 7 Tesla small bore magnet with a 660mT/m gradient insert (Bruker BGA 12-S).

Mice were split into 2 groups of n=5. Group 1 was a time-matched control without MR targeting and Group 2 underwent 1 hour of MR targeting with gradients pulsed 2ms on, 7ms off at 50% total strength (300mT/m); and applied direction selected for coarse steering to the tumor site for the Prostate (−z, −y) (Fig. 2a). For steering to the lungs (+z and −y gradients), the absence of an × gradient should ensure even distribution of magnetic particles in each lung.

The force on magnetically labeled cells is dependent on whether the SPIOs have become magnetically saturated. When unsaturated, the force is dependent on the magnetic susceptibility of the SPIOs, the magnetic field and also the magnetic field gradient[32]. However once the SPIOs reach saturation, the force is no longer dependent on the magnetic susceptibility of the particle but the saturation magnetization and as such only the magnetic field gradient will affect the force applied to the cells[7]. SPIOs typically reach magnetic saturation well below 1T, for example in Riegler et al[6], where the SPIOs become saturated at around 300mT, therefore MRT is feasible on clinical MRI systems provided the same magnetic field gradient is used ~300mT/m.

Following MRI-steering, high-resolution RARE (TR = 4.2s, TE=12ms, RARE factor 8, 512*192, no averaging, 9 slices 1mm thick) and gated FLASH (TR = 8.9ms, TE = 1.2ms, 24 reps, 128*128, FA 15°) images of the tumor (prostate only) were captured using a ^{1}H volume resonator (Bruker, 300MHz, 1kW max, outer diameter 118mm/ inner diameter 72mm). Once complete relaxometry-using MSME (TE 10ms, Echo Spacing 10ms, 16 echoes, TR 2s, matrix size 256*256) and MGE (TE 2.5ms, Echo Spacing 3.7ms, 12 echoes, TR 10s, matrix size 128*128, FA 90°) was performed to assess the transverse relaxation rates. After treatment, animals were sacrificed and tissues including tumors, kidney, liver, lungs and spleen, were either paraffin wax embedded and fixed for immunohistochemistry or analyzed by flow cytometry to determine macrophage uptake (see supplementary files for details).

Vascular permeability

A further study was performed to assess vascular permeability in mice. Mice were administered with 3 million SPIO-loaded MDM one group underwent MR targeting and the other remained in the scanner as described above. Immediately after targeting mice were injected *i.v.* with a 100 ul mixture of FITC-conjugated *Lycopersicon esculentum* (tomato)

Europe PMC Funders Author Manuscripts

Europe PMC Funders Author Manuscripts

lectin (1 mg/ml; Vector Laboratories) and *Ricinus communis* agglutinin I (2.5 mg/ml; Vector Laboratories). Perfusion-fixation with 4% paraformaldehyde was performed 10 min following lectin administration. Harvested tissue was post-fixed in 4% paraformaldehyde, processed through graded sucrose, and embedded in OCT medium (Tissue-Tek). Sections at approximately 40 um were counterstained with DAPI (0.05 mg/ml, Invitrogen) and confocal image stacks were acquired by confocal microscopy (Nikon). Measurement of vascular volumes was performed on images from tumor-bearing mice with and without MRT targeting (n=3 mice/group and 5-10 fields of view).

In addition vasculature leakage was also assessed using the contrast agent gadolinium-diethylenetriaminepentaacetic acid (Gd-DPTA)[31,32]. Mice receiving SPIO-loaded MDM with and without MR targeting were removed from the scanner and injected (via tail vein) with a 0.1mmol/Kg dose of Gd-DPTA (Magnevist) (N=3 mice/group). Mice were then returned to the scanner and T1 weighted imaging (TR=100ms, TE=3.7ms, FA = 30 degs, matrix size=256*256) was performed for 15 minutes (50 repetitions) post injection. Data were used to assess pooling of the contrast agent over time as an indicator of a leaky, damaged vasculature. Experiments were repeated with Gd-DPTA alone (no iron labeled macrophages or MRT). Uptake of Gd-DTPA was monitored in tumour tissue over the 15-minute period; any pooling would result in increased signal over this time period. We also monitored GD-DTPA uptake in the muscle surrounding the spinal cord (vertically away from the −y gradient targeted tumour region) as a control region where we expect no vascular disruption due to MRT. Direct comparisons in changes in signal intensity were made between these two regions to investigate any vascular damage in the targeted region. Finally, if there is no vascular damage Gd-DTPA should enter the renal system; to confirm this in our groups we imaged the kidneys.

Therapeutic studies

HSV1716 in vitro studies are described in the accompanying supplementary file. In vivo studies were performed as follows. Tumor bearing mice received tail vein injections of either 3 million MDM alone or armed with Seprehvir at MOI 50, 1×10^7 Seprehvir only or PBS (n=5 mice/group). Of note, 3 groups of mice were administered MDM +OV, one group underwent MR targeting for 1h, one sat in the MRI scanner but had no MR targeting (MDM +OV no MRT) and another group did not enter the MRI scanner (MDM+OV). Tumor size was monitored by IVIS Lumina II imaging (IVIS, Caliper Life Sciences). Animals were sacrificed once tumors reached the maximum volume ($>10^{10}$ ps-1) permitted by UK Home Office Regulations. Excised tissues including tumors, kidney, liver, lungs, and spleen were embedded in OCT or paraffin wax for immunocytochemical/ histologic labeling studies.

Histological analysis

Tissues were divided into two; one part was formalin fixed for immunohistological analysis and the other was dissected free of adherent fibrous and fatty tissue and treated with collagenase. Flow cytometry: cell viability was determined using LIVE/DEAD Fixable Violet Dead Cell Stain Kit (Invitrogen). All FACS data were analyzed on an LSR II flow cytometer (BD Biosciences) using FlowJo software (Tree Star). **Histology:** Five micron sections of all organs were incubated with specific antibodies for target antigens; for the

Europe PMC Funders Author Manuscripts

Europe PMC Funders Author Manuscripts

vasculature we used CD31 (1:100), (AbD Serotec) and for macrophages human CD68 (Dako, Ely, UK) at 1:100. A biotinylated secondary antibody system was used in conjunction with a streptavidin-conjugated HRP. Peroxidase activity was localised with diaminobenzidine (Vectastain Elite ABC kit, Vector Labs). To detect iron in the tumors (where cell densitites were high) sections were stained with Perls Prussian blue and counter-stained with eosin for improved contrast. To detect cancer cells in the lungs all lung sections were stained with Epithelial cell adhesion molecule (EPCAM) or Hematoxylin and eosin (H&E). All immune-localization experiments were repeated on multiple tissue sections and included isotype-matched controls for determination of background staining. To assess necrosis the area of necrosis within the whole-tumor section was determined visually, and the proportion of necrotic nonviable tumor areas over the whole section was calculated using ImageJ software (National Institute of Health). For each group, the mean percentage of necrosis and standard error were calculated. The results are presented as the mean tumor necrosis (%) for all tumors (five slices per each tumor) in each treatment group.

Immunofluorescence: Harvested tissue was post-fixed in 4% paraformaldehyde, processed through graded sucrose, and embedded in OCT medium (Tissue-Tek) and stored at −80°C. Frozen sections were dried for 10 minutes at room temperature and blocked in 5% horse serum + 0.5% saponin in PBS for 30 minutes. Sections at approximately 4 μm were stained with anti-GFP 1:200 (ab290 abc anti UK) and CD68 (1:100) for 1 hour and then secondary antibodies donkey anti-rabbit alexa fluor 488 and goat anti-mouse 540 at 1:100 dilution (Invitrogen, Paisley, UK) and finally counterstained with prolong gold-antifade mountant with DAPI (4′,6-diamidino-2-phenylindole 0.05 mg/ml, Invitrogen). Images of macrophage infiltration into primary and pulmonary LnCAP tumors were captured using a spinning disc confocal microscope (Olympus IX81, PerkinElmer, UK). Confocal image Z-stacks of tumors were captured at 1μm increments at ×20 magnification.

Statistical analysis

Data are means ± SEM (Prism 5; GraphPad Software). Two-tailed student's *t* test were used to analyze the statistical significance of the data unless otherwise stated. Differences were termed significant with a *P* value of less than 0.05.

Supplementary Material

Refer to Web version on PubMed Central for supplementary material.

Acknowledgments

This work was funded mainly by the Medical Research Council (MRC), UK (grant G0902317/1). CEL also acknowledges the support of the CRUK (grant C11712/A13028). ML receives funding from Medical Research Council (grant MR/J013110/1); the King's College London and UCL Comprehensive Cancer Imaging Centre CR-UK & EPSRC, in association with the MRC and DoH (England); the National Centre for the Replacement, Reduction and Refinement of Animal in Research (NC3Rs); UK Regenerative Medicine Platform Safety Hub (MRC: MR/K026739/1); and Eli Lilly and Company. We thank Dr Johannes Riegler for his support during this project.

References

1. Syed BA, Evans JB. Stem cell therapy market. Nature reviews. Drug discovery. 2013; 12:185–186. doi:10.1038/nrd3953.

Europe PMC Funders Author Manuscripts

2. Kyrtatos PG, et al. Magnetic tagging increases delivery of circulating progenitors in vascular injury. JACC. Cardiovascular interventions. 2009; 2:794–802. [PubMed: 19695550]
3. Arbab AS, et al. In vivo trafficking and targeted delivery of magnetically labeled stem cells. Human gene therapy. 2004; 15:351–360. [PubMed: 15053860]
4. Riegler J, et al. Targeted magnetic delivery and tracking of cells using a magnetic resonance imaging system. Biomaterials. 2010; 31:5366–5371. [PubMed: 20382425]
5. Landazuri N, et al. Magnetic targeting of human mesenchymal stem cells with internalized superparamagnetic iron oxide nanoparticles. Small. 2013; 9:4017–4026. [PubMed: 23766267]
6. Riegler J, et al. Superparamagnetic iron oxide nanoparticle targeting of MSCs in vascular injury. Biomaterials. 2013; 34:1987–1994. [PubMed: 23237516]
7. Muthana M, et al. A novel magnetic approach to enhance the efficacy of cell-based gene therapies. Gene Ther. 2008
8. Yellen BB, Hovorka O, Friedman G. Arranging matter by magnetic nanoparticle assemblers. Proc Natl Acad Sci U S A. 2005; 102:8860–8864. [PubMed: 15956215]
9. Martel, S., et al. Medical and technical protocol for automatic navigation of a wireless device in the carotid artery of a living swine using a standard clinical MRI system. Medical image computing and computer-assisted intervention: MICCAI … International Conference on Medical Image Computing and Computer-Assisted Intervention; 2007; p. 144-152. 10
10. Chanu, A.; Martel, S. Real-time software platform design for in-vivo navigation of a small ferromagnetic device in a swine carotid artery using a magnetic resonance imaging system; Conference proceedings: … Annual International Conference of the IEEE Engineering in Medicine and Biology Society. IEEE Engineering in Medicine and Biology Society. Conference; 2007; p. 6585-6588.
11. Surder D, et al. Cell-based therapy for myocardial repair in patients with acute myocardial infarction: rationale and study design of the SWiss multicenter Intracoronary Stem cells Study in Acute Myocardial Infarction (SWISS-AMI). American heart journal. 2010; 160:58–64. [PubMed: 20598973]
12. Kim BG, Hwang DH, Lee SI, Kim EJ, Kim SU. Stem cell-based cell therapy for spinal cord injury. Cell transplantation. 2007; 16:355–364. [PubMed: 17658126]
13. Garbayo E, et al. Neuroprotective properties of marrow-isolated adult multilineage-inducible cells in rat hippocampus following global cerebral ischemia are enhanced when complexed to biomimetic microcarriers. Journal of neurochemistry. 2011; 119:972–988. [PubMed: 21496021]
14. Biju KC, et al. Bone marrow-derived microglia-based neurturin delivery protects against dopaminergic neurodegeneration in a mouse model of Parkinson's disease. Neuroscience letters. 2013; 535:24–29. [PubMed: 23295906]
15. Magga J, et al. Production of monocytic cells from bone marrow stem cells: therapeutic usage in Alzheimer's disease. Journal of cellular and molecular medicine. 2012; 16:1060–1073. [PubMed: 21777378]
16. De Palma M, et al. Tumor-targeted interferon-alpha delivery by Tie2-expressing monocytes inhibits tumor growth and metastasis. Cancer cell. 2008; 14:299–311. [PubMed: 18835032]
17. Muthana M, et al. Use of macrophages to target therapeutic adenovirus to human prostate tumors. Cancer Res. 2011; 71:1805–1815. [PubMed: 21233334]
18. Muthana M, et al. Macrophage Delivery of an Oncolytic Virus Abolishes Tumor Regrowth and Metastasis After Chemotherapy or Irradiation. Cancer Res. 2013
19. Kandalaft LE, Powell DJ Jr. Coukos G. A phase I clinical trial of adoptive transfer of folate receptor-alpha redirected autologous T cells for recurrent ovarian cancer. J Transl Med. 2012; 10:157. [PubMed: 22863016]
20. Kershaw MH, et al. A phase I study on adoptive immunotherapy using gene-modified T cells for ovarian cancer. Clin Cancer Res. 2006; 12:6106–6115. [PubMed: 17062687]
21. Engell-Noerregaard L, Hansen TH, Andersen MH, Thor Straten P, Svane IM. Review of clinical studies on dendritic cell-based vaccination of patients with malignant melanoma: assessment of correlation between clinical response and vaccine parameters. Cancer Immunol Immunother. 2009; 58:1–14. [PubMed: 18719915]

Europe PMC Funders Author Manuscripts

22. Bartholeyns J, Lopez M, Andreesen R. Adoptive immunotherapy of solid tumors with activated macrophages: experimental and clinical results. Anticancer Res. 1991; 11:1201–1204. [PubMed: 1888150]

23. Bartoleyns J, Romet-Lemonne JL, Chokri M, Lopez M. Immune therapy with macrophages: present status and critical requirements for implementation. Immunobiology. 1996; 195:550–562. [PubMed: 8933156]

24. Studeny M, et al. Bone marrow-derived mesenchymal stem cells as vehicles for interferon-beta delivery into tumors. Cancer Res. 2002; 62:3603–3608. [PubMed: 12097260]

25. Leek RD, Landers RJ, Harris AL, Lewis CE. Necrosis correlates with high vascular density and focal macrophage infiltration in invasive carcinoma of the breast. Br J Cancer. 1999; 79:991–995. [PubMed: 10070902]

26. Burke B, et al. Hypoxia-induced gene expression in human macrophages: implications for ischemic tissues and hypoxia-regulated gene therapy. Am J Pathol. 2003; 163:1233–1243. [PubMed: 14507633]

27. Nakasone ES, et al. Imaging tumor-stroma interactions during chemotherapy reveals contributions of the microenvironment to resistance. Cancer cell. 2012; 21:488–503. [PubMed: 22516258]

28. Branca RT, et al. Molecular MRI for sensitive and specific detection of lung metastases. Proc Natl Acad Sci U S A. 2010; 107:3693–3697. [PubMed: 20142483]

29. Sorensen A, et al. In vivo evaluation of a cancer therapy strategy combining HSV1716-mediated oncolysis with gene transfer and targeted radiotherapy. Journal of nuclear medicine: official publication, Society of Nuclear Medicine. 2012; 53:647–654.

30. Setsompop K, et al. Pushing the limits of in vivo diffusion MRI for the Human Connectome Project. NeuroImage. 2013; 80:220–233. [PubMed: 23707579]

31. Beauregard DA, Hill SA, Chaplin DJ, Brindle KM. The susceptibility of tumors to the antivascular drug combretastatin A4 phosphate correlates with vascular permeability. Cancer Res. 2001; 61:6811–6815. [PubMed: 11559555]

32. Pike MM, et al. High-resolution longitudinal assessment of flow and permeability in mouse glioma vasculature: Sequential small molecule and SPIO dynamic contrast agent MRI. Magnetic resonance in medicine: official journal of the Society of Magnetic Resonance in Medicine / Society of Magnetic Resonance in Medicine. 2009; 61:615–625.

Europe PMC Funders Author Manuscripts

Europe PMC Funders Author Manuscripts

Europe PMC Funders Author Manuscripts

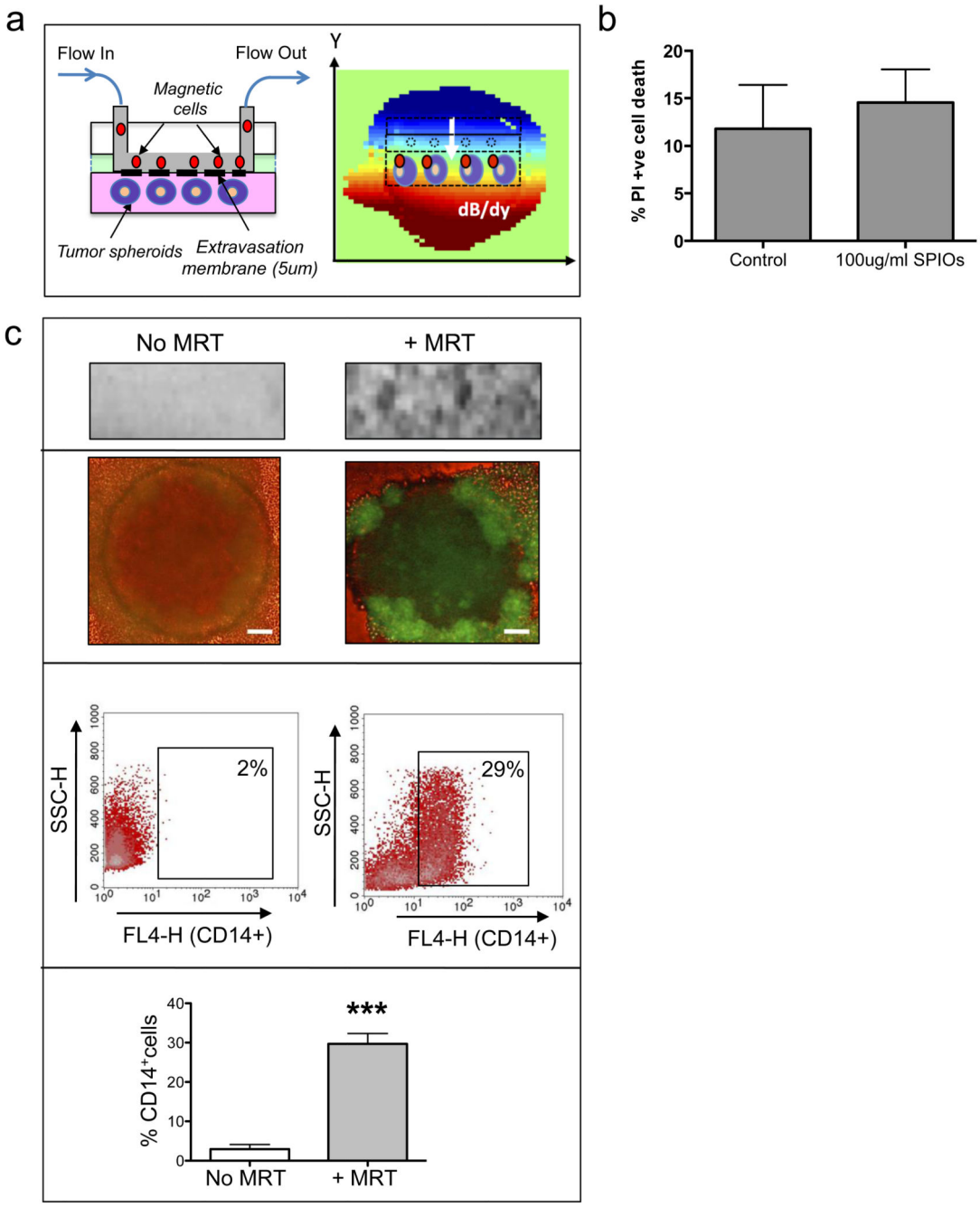

Figure 1. MRT using a novel trans-endothelial migration (TEM) flow assay

We have designed a flow chamber that can accommodate 3D tumor spheroids as well as a vascular endothelial layer. The flowing 'magnetic cells' will therefore need to cross the vascular barrier before entering a 3D tumor simulating the passage of cells across endothelial cells in a blood vessel wall (a: left panel). The TEM flow chamber is placed in the iso-centre of an MRI scanner with a spherical (6mm diameter) homogenous 7T magnetic field. We applied a pulsed gradient (50% of max) with strength of 300mT/m in the (−y) gradient direction. The resulting heterogeneous magnetic field (dB/dy field) can steer

magnetic particles towards the tumor spheroids for increased uptake (a: right panel). Cell viability following SPIO uptake was not compromised as assessed by flow cytometry for propidium iodide uptake (b). Uptake was confirmed by a distortion in the MRI image and a loss of signal compared to when no MRT was applied (c, upper panel). Corresponding fluorescent images of wholes spheroids infiltrated with macrophages carrying a reporter adenovirus (AdCMVGFP) are shown in (c, 2nd panel). Bars = 100μm. Flow cytometry of enzymatically dispersed spheroids revealed that the number of magnetic-cells infiltrating spheroids (% of all cells present in spheroids that were CD14+) was significantly increased when a gradient was applied (c, lower panels). All images and data (means ± SEM) are derived from 6 independent experiments. Comparisons between groups were performed using two-tailed unpaired Student's t-test $p = 0.0001$, compared with No MRT group.

Europe PMC Funders Author Manuscripts

Europe PMC Funders Author Manuscripts

Europe PMC Funders Author Manuscripts

Europe PMC Funders Author Manuscripts

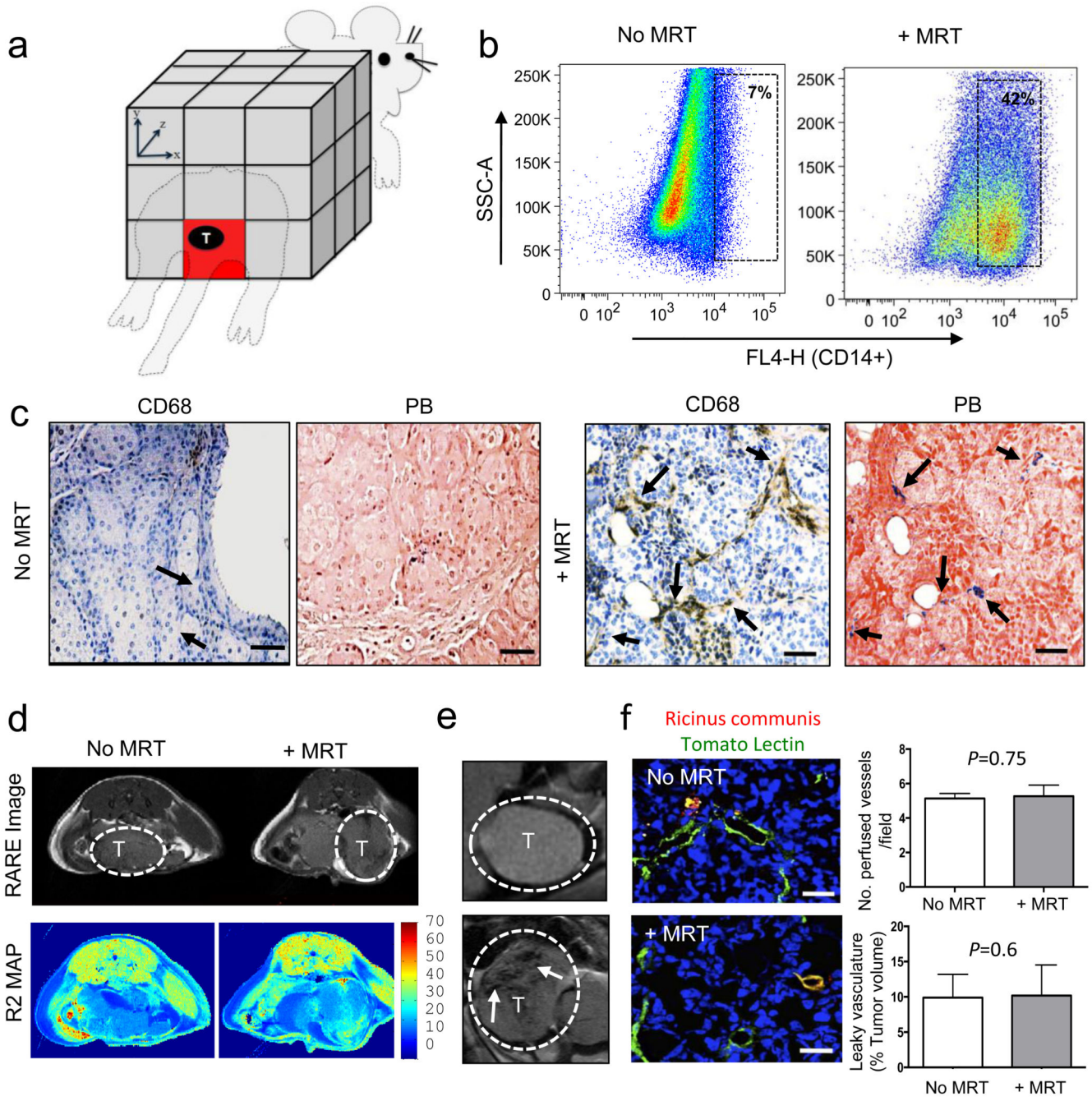

Figure 2. Magnetic macrophages were steered into primary prostate tumors using MRT

(a) Schematic of targeted regions using imaging gradients for MR Targeting. We applied a −Y gradient applied equally across the animal to target the location of the prostate as depicted (red box). Three million magnetically labelled macrophages were then administered to mice via i.v. injection and anesthetised mice were then placed into the isocentre of a 7T MRI scanner. Subjects were split into 2 groups with n=5 mice/group. Group 1 were imaged after 1 hour (no MR Targeting). Group 2 underwent MRI targeting. Post mortem we confirmed the increased levels of human macrophage uptake by (b) FACS

analysis of collagenase-treated tumors one hour after MRI targeting, and (c) histological staining of paraffin wax-embedded tumor sections with an anti-human CD68 antibody and Prussian blue (CD68 positive macrophages are brown and SPIO positive macrophages are blue: see arrows). Representative RARE images from 5 mice/group and R2 maps for each group are shown (d) and (e). T=Tumor, bars= 200μm. (f) The number of perfused vessels in tumors in mice who underwent MRT compared to mice with no MRT was determined by perfusion with tomato lectin (green). Arrows point to areas vascular leakage. Mean ± SEM, p=0.75, Student's t test; analysis of tumors from n=5 mice per group and 5–10 fields of view (FOV) per tumor. The total volume of leaky vasculature does not differ between tumors in the two groups of mice (mean ± SEM; p=0.6, Student's t test; analysis of tumors from 3 mice per group and 5–10 FOV per tumor). Bar= 34μm.

Europe PMC Funders Author Manuscripts

Europe PMC Funders Author Manuscripts

Europe PMC Funders Author Manuscripts

Europe PMC Funders Author Manuscripts

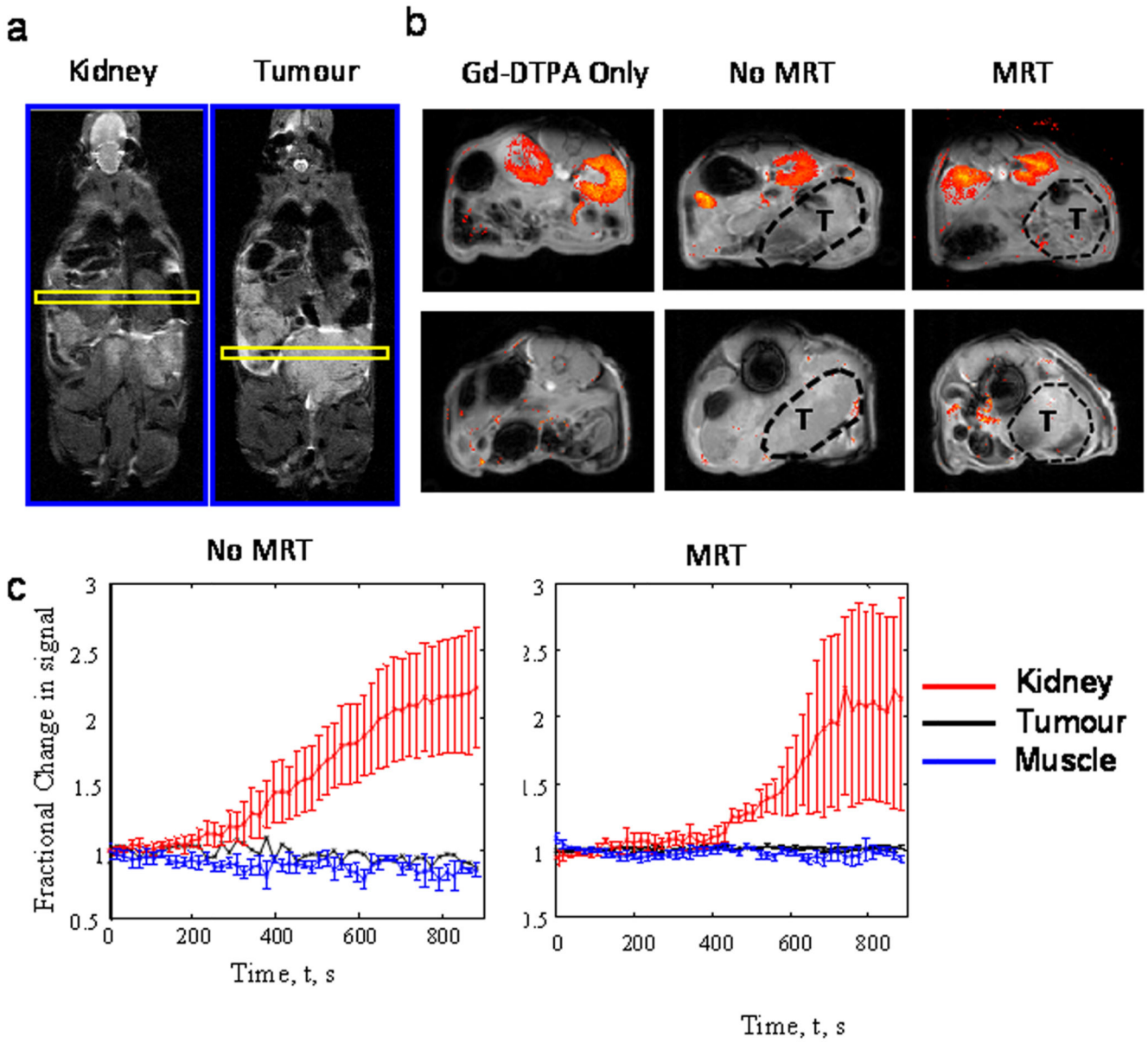

Figure 3. MR targeting of magnetic cells into tumors does not affect vasculature

Representative maps of Gadolinium pooling are shown for each group of mice where n=3 mice/group. The position of the slices (yellow) from which the MRI images were taken is shown - one for the kidneys and the other the tumour (a). In all cases the T1 weighted images show higher signal intensity in the kidneys (b; upper panel) than in the prostate tumors (b; lower panel), where gadolinium pooled within the urinary system of the mice following administration. (c) Regions of interest were taken in kidney, tumour and muscle tissue and time series analysis of contrast agent pooling is shown for the MRT group and time matched 'no MRT' group. Both muscle and tumour tissue show no apparent change in MR signal intensity over time compared to the kidney, providing further evidence that the vasculature has remained intact following MRT therapy. All data are means ± SEM from n=3 mice/group.

Europe PMC Funders Author Manuscripts

Europe PMC Funders Author Manuscripts

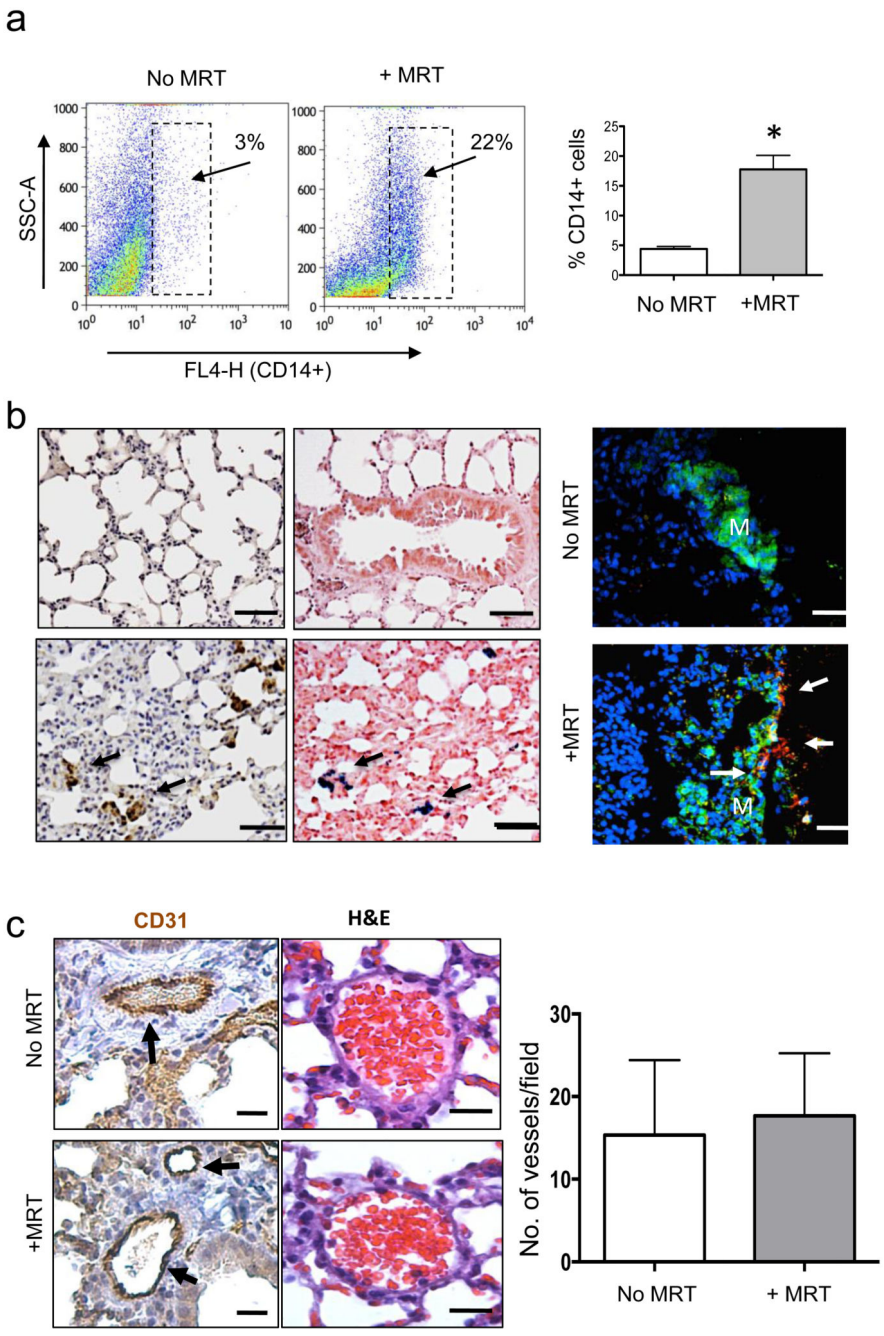

Figure 4. Magnetic macrophages were steered into pulmonary metastasis using MRT

Short-pulsed magnetic gradients were used to steer SPIO-loaded macrophages towards the lungs. (a) FACS analysis of collagenase-treated lungs showed significantly more human CD14+ macrophages were present in lungs with than without MR targeting. Analysis of tumors from n=3 mice per group where data are mean ± SEM, student's t test *, $P < 0.01$ compared with non-MR targeted lungs. (b) Representative images from n=3 mice/group are shown, this revealed increased immunostaining for human CD68 and Prussian blue in lung sections (CD68+ cells are brown and SPIO+ cells blue: see arrows). Bar = 75μm. This was

Europe PMC Funders Author Manuscripts

Europe PMC Funders Author Manuscripts

also confirmed in immunofluorescence stained sections using an anti-GFP antibody/green and CD68/red (bar = 75μm, M=metastasis and arrows point to CD68+ve cells) (c) Immunostaining with CD31 (Bar= 50μm) and H&E (Bar=200μm) indicated that MR targeted delivery of magnetic macrophages into the lungs had no adverse affects on the lung vasculature compared to delivery without targeting. Representative data are shown from one of two replicate experiments in which n=3 mice/group. SEMs are depicted and student t-test $P < 0.75$ compared MR targeted with non-MR targeted lungs.

Europe PMC Funders Author Manuscripts

Europe PMC Funders Author Manuscripts

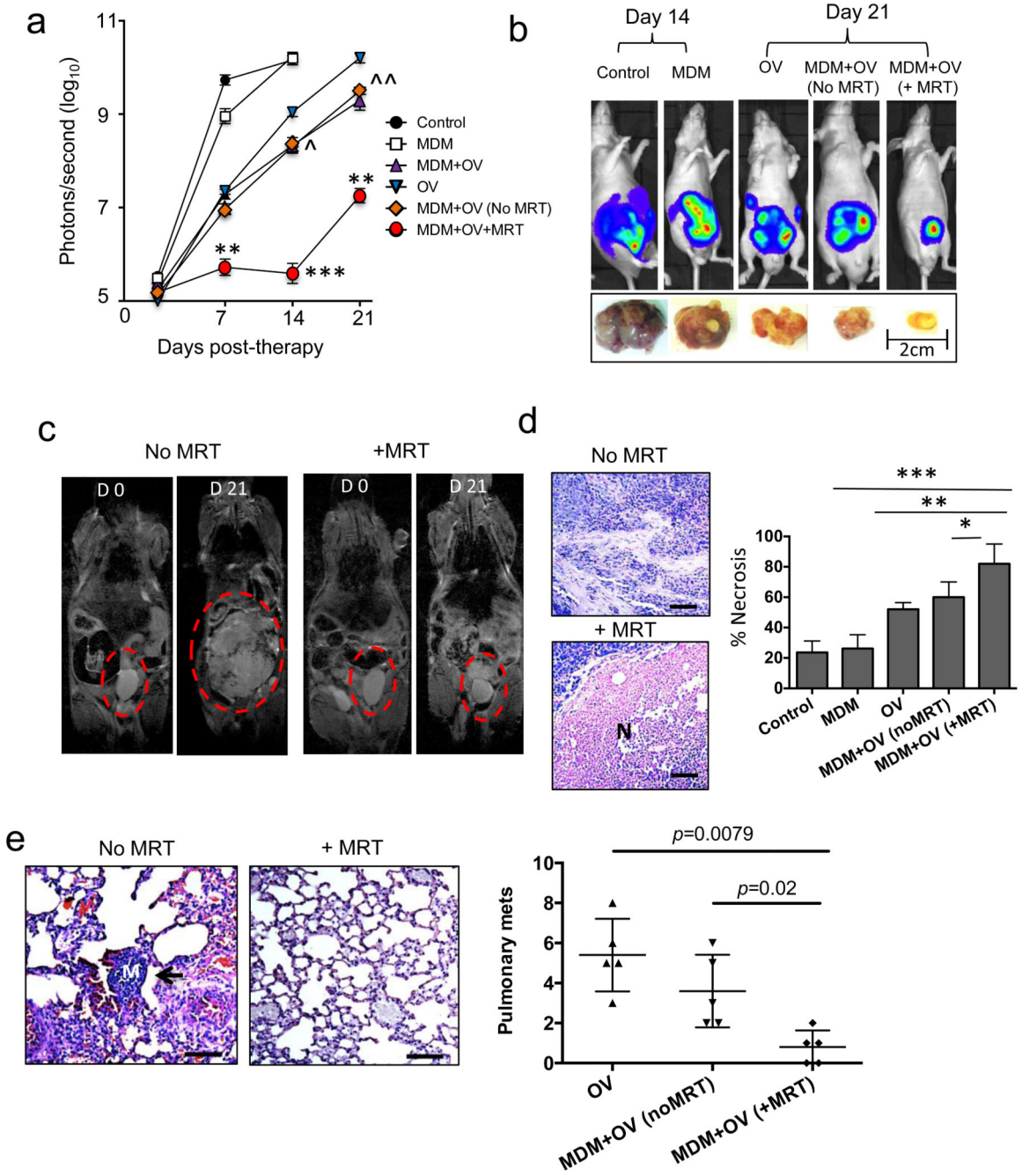

Figure 5. Magnetic targeting increases the anti-tumor effects of oncolytic macrophage

Tumor-bearing mice were administered with a single dose of human monocyte-derived macrophages (MDM) carrying the oncolytic virus, HSV1716 (MDM+OV). These were divided into three groups of mice (each with 5 mice/group). One group underwent MR targeting to either the prostate gland or lungs (MDM+OV+MRT) for 1 h, another was exposed to the MRI scanner but with no MR targeting (MDM+OV no MRT) and the third (MDM+OV) did not enter the MRI scanner. Additional groups of mice received 100ul of PBS (Control), a single dose of 1×10^7 pfu HSV1716 (OV) or 3 million untreated MDM.

Mice were imaged weekly using the IVIS imaging system and, after 21 days, tumors and lungs were removed and processed for histology. (a) Tumor luminosity in n=5 mice/group showed MR Targeting significantly improved the effect of OV-MDM on tumor growth (b) Representative IVIS images and photographs of primary tumors following various treatments (c) Representative RARE images for MDM+OV with or without MR targeting show marked difference in tumor size at the beginning and end of therapy. Representative images of H&E stained sections from n=5 mice/group show (d) the area of necrosis (N) in primary tumors and (e) the number of metastases (see arrow, M=Metastasis) in the lungs of mice receiving MDM+OV with or without MR targeting Bars in panels d-e= 200 μm. Data shown are means ± SEMs of n=5 mice/group. For the lung metastasis quantitative analysis was carried out on 10 high-power fields (HPF; ×20 magnification) per tissue section. Comparisons between more than two groups were performed using one-way ANOVA followed by post-hoc Bonferroni test. *P < 0.05; **P < 0.001; ***P < 0.0001 compared with MDM+OV+MRT to MDM+OV (no MR targeting) and ^ is comparing MDM+OV (no MR targeting) and free OV group.

Europe PMC Funders Author Manuscripts

Europe PMC Funders Author Manuscripts

Europe PMC Funders Author Manuscripts

Europe PMC Funders Author Manuscripts

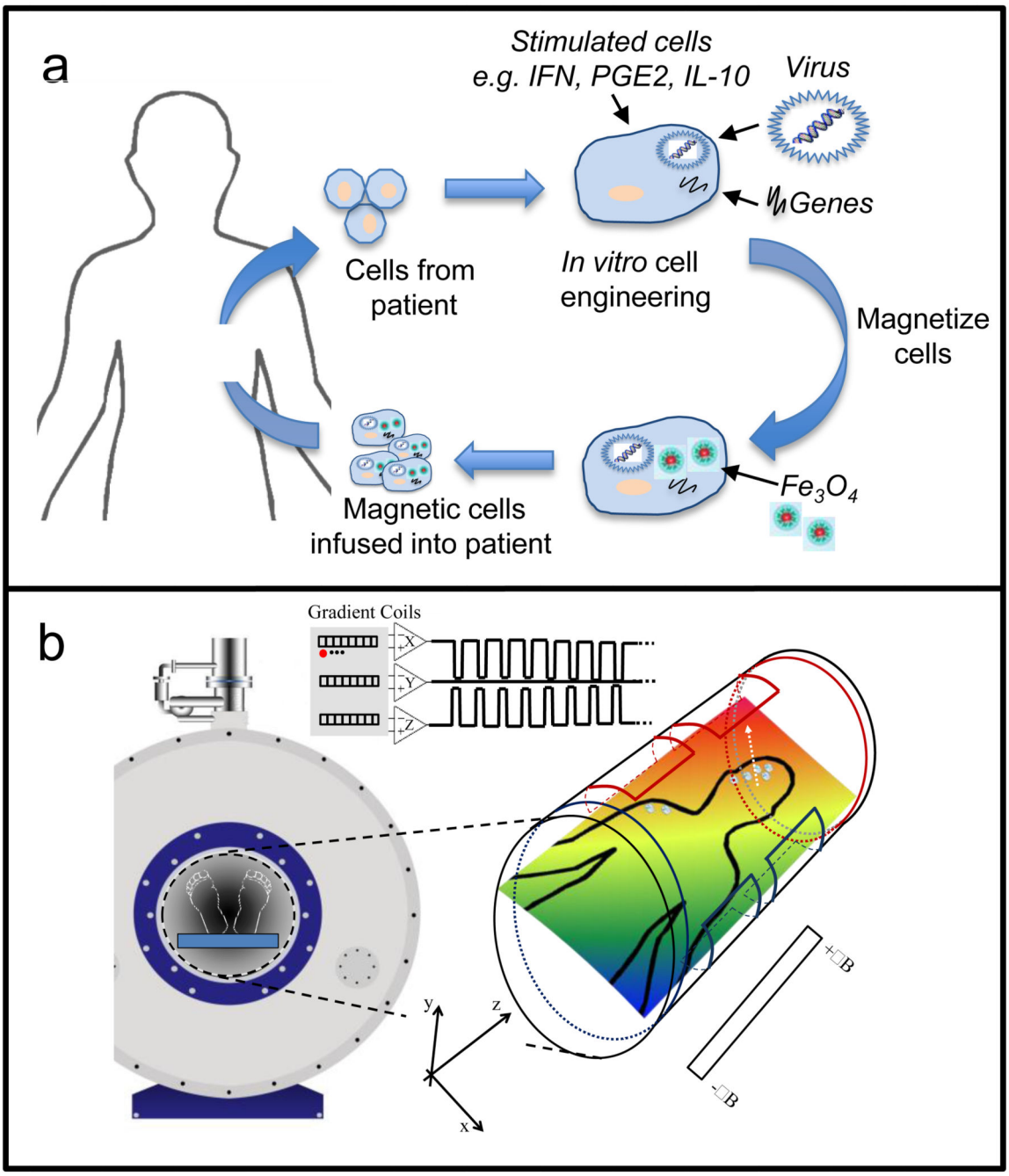

Figure 6. Principle of MR targeting to steer cell-based therapies to specific tissues

(a) The cells used for these studies are derived from monocytes isolated from patient blood. These cells are cultured in the presence of various stimuli to produce 'therapeutic' macrophages (e.g. cytokines, therapeutic genes or viruses) and loaded with SPIOs before re-infusion back into the same patient. (b) The subject is then placed in the centre of an MRI scanner where linear spatial encoding magnetic gradients can be used to induce a force on a magnetized body. The magnetic cells injected into the bloodstream of the subject circulate and are targeted into the diseased organ/tissue under the influence of the applied magnetic

field. Field map plots demonstrate that significant field gradients can be generated in various directions by the MRI gradient coils. The resulting magnetic field (dB/dy field) can steer magnetic cells towards the diseased tissue for increased cell uptake.

Europe PMC Funders Author Manuscripts

Europe PMC Funders Author Manuscripts